

Characteristics analysis of a combined system of vacuum membrane distillation and mechanical vapor recompression

Zetian Si, Dong Han*, Jiming Gu, Yan Song, Pengpeng Zhang

Nanjing University of Aeronautics and Astronautics, College of Energy and Power Engineering, Energy Conservation Research Group (ECRG), Nanjing, Jiangsu 210016, China, emails: handong@nuaa.edu.cn (D. Han), tian3221623@126.com (Z. Si), Gujiming@nuaa.edu.cn (J.M. Gu), 1121523091@qq.com (Y. Song), 3188812179@qq.com (P.P. Zhang)

Received 19 January 2019; Accepted 11 August 2019

ABSTRACT

Vacuum membrane distillation (VMD) is the efficient method to evaporate freshwater from aqueous solution. However, energy requirement in the distillation process still remains as the biggest obstacle. In this paper, a new combined system with VMD and mechanical vapor recompression subsystems coupled for the concentration of sodium chloride solution is proposed, to reduce the energy consumption of evaporation by recovering latent heat from the compression process. In light of the thermal processes included, mathematical models were established based on the mass and energy balance equations. The influences of the operating parameters on temperature and concentration polarization effects are investigated. The mechanisms of influencing compressor power from the appointed key factors such as, temperature polarization effect, concentration polarization effect and boiling point elevation (BPE) and so on, at various operating conditions are revealed. The simulation results present that the power consumption of compressor can be reduced appropriately through weakening the impacts of temperature and concentration polarization effects and BPE on distillation process by adjusting operating conditions. Moreover, the specific thermal energy consumption is found to be 85 kWh/m³, which is about 39.3% lower than that of the solar powered membrane distillation system.

Keywords: Vacuum membrane distillation; Mechanical vapor recompression; Temperature polarization effect; Concentration polarization effect; Boiling point elevation; Compressor power

1. Introduction

Together with the energy supply and environmental protection, fresh water production is one of the three critical elements for the sustainable development of every country in the world. At present, the lack of fresh water seriously threatens the lives of people in many remote and arid areas, owing to over-population, climate change, accelerating development of industrialization, and environmental pollution. Thus, supplying fresh water to these places is one of the greatest challenges. Alternatives such as brackish and seawater desalination become an available option for the providing of freshwater supplies. Over the years various

commercial technologies for desalination have been developed including membrane separation processes such as electrodialysis, nanofiltration and reverse osmosis, as well as thermal distillation, multistage flash, multiple effect evaporation and vapor compression distillation [1,2]. However, among these conventional desalination technologies, the cost and energy consumption impose as a main barrier for the remote and arid areas to adopt desalination as the primary resource of fresh water, which have forced researchers and scholars to look for an alternative way of seawater desalination.

As a relatively new desalination technology in recent years, membrane distillation (MD) has received increasing

* Corresponding author.

attention due to the advantages of the gentle operating conditions, and simple technological process. The principle of MD process is based on the evaporation through microporous hydrophobic membrane, which is employed as a barrier separating heated feed phase and cold permeate phase [3]. The pore size should be enough small so that only the evaporated water vapor molecules can pass through the membrane pores under the driving force by partial vapor pressure difference on both sides of the membrane. Up to now, MD can be classified into four types of configurations depending on the methods of vapor condensation in the permeate side: direct contact membrane distillation (DCMD), air gap membrane distillation, sweeping gas membrane distillation (SGMD), vacuum membrane distillation (VMD). Because of creating a vacuum atmosphere in the permeate side, the VMD exhibits the highest driving force and membrane flux amongst the above-mentioned types [4]. Extensive studies for MD applications have been carried out all over the world. Tijjing et al. [5] conducted experiments using DCMD system for desalination, it was found that the system had a high membrane flux of 30 kg/(m² h) when the concentration of sodium chloride solution was 35 g/L. Khayet et al. [6] proposed a central compositional orthogonal design for modeling and optimization of the SGMD process, and investigated the influences of operating conditions on membrane flux. Finally, the operating parameters for optimum performance of membrane flux and energy consumption were obtained. Shao et al. [7] conducted an experimental and theoretical researches about the concentration of N-methyl-2-pyrrolidone aqueous solution by means of VMD module, which was made from polypropylene hollow fiber membrane, the author found that the membrane flux and the rejection could reach 9.5 kg/(m² h) and 98%, respectively, at the feed temperature of 80°C and permeate-side absolute pressure of 10 kPa.

However, due to the lower membrane flux and thermal efficiency, the commercial application of MD technology is limited seriously. Therefore, several researchers have also focused on new MD membranes materials with higher mass transfer coefficient aiming to improve membrane flux. Chen et al. [8] investigated the structure and performance of VMD module made from Polyvinylidene fluoride composite membranes by the nonsolvent induced phase separation technique. Mendez et al. [9] believed that the membrane flux could be increased by changing the membrane materials performances and process design in the process of seawater desalination by MD, especially highly permeable and thin dense self-standing membranes could be used effectively to avoid membrane wetting, resulting in increasing membrane flux. Zhang et al. [10] experimentally studied the effects of SiO₂ concentration on the membrane parameters in the VMD process using the hydrophobic asymmetric SiO₂-PDMS-PVDF hollow fiber membranes, the results show that the prepared hydrophobic asymmetric SiO₂-PDMS-PVDF membranes have good anti-wetting property, stability and high permeability. However, other researchers tried to optimize the process through looking for the optimal operation parameters or by coupling with other processes. Banat et al. [11] investigated a DCMD module with solar collector system for desalination. The obtained results showed that the specific thermal energy consumption (STEC) was in the

range of 200–300 kWh/t which was lower than the conventional MD system (640 kWh/t). Ma et al. [12] designed an integrated system coupling VMD and solar flat-plate collector for seawater desalination, the simulation results showed that the gained output ratio can be above 0.7. Although, the integration of solar energy into the MD process could significantly reduce the energy consumption and production cost, it could not achieve continuous and stable production of fresh water because the solar heating system is strongly dependent on climate conditions. Consequently, Boutikos et al. [13] proposed a new multi-effect VMD system based on the principle of steam latent heat recovery in the multi-effect evaporation process, the STEC was found to be 250 kWh/t when the feed flow rate and feed temperature were maintained at 120 L/h and 80°C, respectively. Practically, there are some limitations on the improvement of energy efficiency in multi-effect VMD process due to complex technological process, lower secondary steam temperature and lower heat transfer temperature difference.

From the above literature reviews, it is found that the existing MD processes generally have the problems of low membrane flux, high energy consumption and low latent heat recovery efficiency. Mechanical vapor recompression (MVR) is a high-efficiency energy-saving method based on the theory of self-heat recuperation [14], which is driven by electric energy, the secondary steam produced by the evaporator is compressed and heated through the steam compressor, and then returns to the evaporator to condense and release the latent heat, thus saving the utilization of fresh steam and cooling circulating water and making full use of the latent heat of the secondary steam. MVR has been widely used in water desalination, drying, evaporation, crystallization and other fields.

In this study, taking the energy saving characteristic of MVR and the advantages of efficient separation and excellent anti-corrosion of MD into account, a new combined system of VMD and MVR for desalination is proposed. Careful integration of VMD in MVR process can be considered to achieve great change in energy efficiency. Mathematical models based on the mass and energy balance of the system are established and validated. The temperature polarization coefficient (TPC) and concentration polarization coefficient (CPC) are calculated to assess the influence of corresponding operating parameters such as feed temperature, feed velocity, feed concentration and permeate-side absolute pressure on temperature polarization effect and concentration polarization effect. Furthermore, the mechanisms of influencing compressor power from the appointed key factors such as temperature polarization effect, concentration polarization effect, boiling point elevation (BPE) and so on, at various operating conditions are revealed, and the matching characteristics of them are discussed more comprehensively. The research method as well as the obtained results lay a good foundation for the following experimental study of the combined system of VMD and MVR.

2. Theory and methodology

2.1. System description

The arrangement of the combined system of VMD and MVR is shown in Fig. 1. The system mainly consists of feed

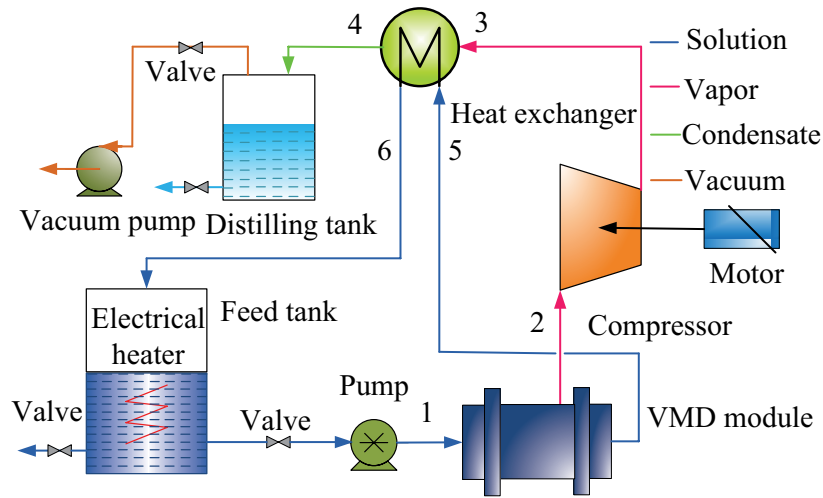


Fig. 1. Schematic diagram of system.

tank, electrical heater, VMD module, steam compressor, heat exchanger, vacuum pump and other auxiliary equipment. The VMD module is composed of hollow fiber membrane tubes, and each tube is made from polytetrafluoroethylene membranes, the structure of VMD module is presented in Fig. 2 and several important parameters are shown in Table 1. The electrical heater is used to preheat the initial aqueous solution to a required temperature in the feed tank, then the preheated solution is pumped to the lumen side of the hollow fibers by a circulating pump, while vacuum is applied at the shell side of the hollow fibers to create a driving force for transmembrane flux by a vacuum pump. Under the driving force created by pressure difference on both sides of the membrane, the water will be vaporized close to the membrane surface and then pass as vapors through the membrane pores. After being evaporated in the VMD module, the feed solution flows to the heat exchanger to be heated again. The generated vapors are compressed by the steam compressor and then put into the heat exchanger to exchange heat with the feed solution, and finally release the latent heat to condense into liquid water which is collected into the distilling tank. The heated solution is directed back

to the feed tank at elevated temperature in order to realize the continuous operation.

2.2. Mathematical models

Taking the sodium chloride solution as the investigation object, the mathematical models are established based on the mass and energy balance equations in order to analyze the relevant thermal performance of the proposed system, the following assumptions and simplifications are applied [15–18]:

- The system works under steady-state conditions.
- The energy losses of the VMD module, heat exchanger and compressor are neglected.
- The power consumptions of circulating pump and vacuum pump are neglected.
- The influence of the non-condensable gas in the system is neglected.
- The solute is no volatilization in evaporation process.
- The compression process of the compressor is adiabatic compression.
- Pressure losses in piping are neglected.

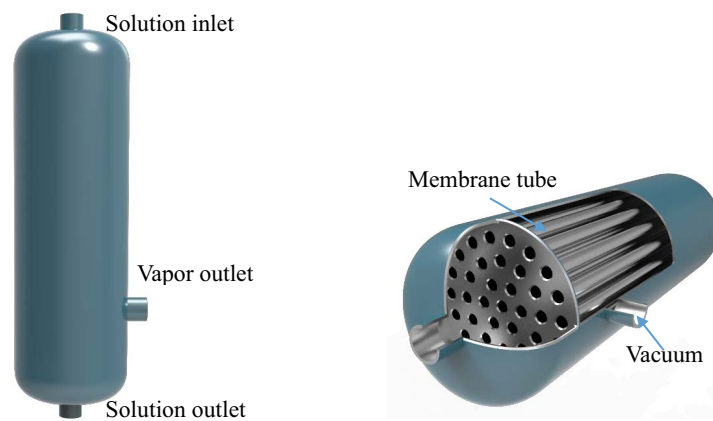


Fig. 2. Structure of VMD module.

Table 1
Parameters of VMD module

Parameters	Values
Pore size (um)	0.2
Inner fiber diameter (mm)	1.8
Outer fiber diameter (mm)	2.6
Porosity (%)	80
Fiber length (m)	0.8
Number of fibers	684
Thickness (mm)	0.4
Effective membrane area (m ²)	3.1

- The condensed water leaving the heat exchanger is saturated.
- The membrane fouling and wetting of VMD module are neglected.

2.2.1. VMD module

The mass balance for the VMD module can be written as follows:

$$F_1 = F_2 + F_5 \quad (1)$$

$$F_1 x_1 = F_5 x_5 \quad (2)$$

where F_1 , F_2 and F_5 are the mass flow rate of the inlet solution, the outlet vapor and the outlet solution, x_1 and x_5 are the solute mass concentration of the inlet and outlet solution.

The energy balance for the VMD module can be written as follows:

$$F_1 h_1 = F_2 h_2 + F_5 h_5 \quad (3)$$

where h_1 , h_2 and h_5 are the specific enthalpy of the inlet solution, the outlet vapor and the outlet solution.

The mass and heat transfer take place simultaneously in VMD process. The transport process in VMD mainly includes the following four steps: (1) Water molecules and heat transfer from the bulk solution to the membrane surface through the boundary layer. (2) Water molecules absorb the heat and evaporate at the membrane surface. (3) Evaporated vapors diffuse through the membrane pores. (4) Vapors with latent heat are taken away and condensed in the condenser outside the membrane module.

2.2.1.1. Heat transfer

The heat transfer within the hot side the boundary layer (Q_f) and the heat transfer across the membrane (Q_m) can be calculated by the following equations. It must be pointed out that the heat transfer across the membrane includes the latent heat associated with the evaporation process and heat transfer through conduction by the membrane.

$$Q_f = h_f A_f (T_f - T_{fm}) \quad (4)$$

$$Q_m = N \Delta H A_{fm} + \frac{k_m}{\delta} A_{fm} (T_{fm} - T_{pm}) \quad (5)$$

$$T_f = \frac{T_1 + T_5}{2} \quad (6)$$

$$A_f = n \pi d l \quad (7)$$

$$A_{fm} = n \pi \frac{D-d}{\ln \frac{D}{d}} l \quad (8)$$

where d , D , l , and n are the inner fiber diameter, outer fiber diameter, fiber length and number of fibers, respectively. A_f is the effective area of inner surface of hollow fiber membrane, A_{fm} is the effective heat transfer area across the membrane, T_f is the feed bulk solution temperature, T_{fm} is the membrane surface temperature, N is the membrane flux, ΔH is the latent heat of evaporation, T_{pm} is the temperature at the permeation membrane surface, k_m is the membrane thermal conductivity, which can be described as:

$$k_m = \varepsilon k_g + (1 - \varepsilon) k_p \quad (9)$$

where k_g and k_p are the thermal conductivity of the gas mixture and membrane material, ε is the porosity of membrane.

The heat transfer coefficient (h_f) at the hot feed solution boundary layer can be calculated by Nusselt equation [19]:

$$\frac{h_f d}{\lambda} = Nu \quad (10)$$

$$Re = \frac{v d \rho}{\mu} \quad (11)$$

$$Pr = \frac{C_p \mu}{\lambda} \quad (12)$$

where ρ , λ , C_p and μ are the density, thermal conductivity, heat capacity and dynamic viscosity of the hot feed solution, respectively. Re is the Reynolds, Pr is the Prandtl numbers, Nu is the Nusselt numbers depending on the flow state of the bulk solution.

For laminar flow, $Re < 2,300$, Nu is given by

$$Nu = 3.66 + \frac{0.0668 \times Re \times Pr \times \frac{d}{l}}{1 + 0.045 \times \left(Re \times Pr \times \frac{d}{l} \right)^{\frac{2}{3}}} \quad (13)$$

For transitional flow, $2,300 < Re < 10,000$, Nu is given by

$$Nu = 0.116 \times \left(Re^{\frac{2}{3}} - 125 \right) \times Pr^{\frac{1}{3}} \times \left(1 + \left(\frac{d}{l} \right)^{\frac{2}{3}} \right) \times \left(\frac{\mu_f}{\mu_{fm}} \right)^{0.14} \quad (14)$$

For turbulent flow, $Re > 10,000$, Nu is given by

$$\text{Nu} = 0.027 \times \text{Re}^{\frac{4}{5}} \times \text{Pr}^{\frac{1}{3}} \times \left(\frac{\mu_f}{\mu_{\text{fm}}} \right)^{0.14} \quad (15)$$

Here, the heat transfer through conduction by the membrane has been neglected [20], and T_{fm} and T_{pm} are almost equal. Therefore, the energy balance equation in heat transfer process is expressed as follows:

$$Q_f = Q_m = h_f A_f (T_f - T_{\text{fm}}) = N \Delta H A_{\text{fm}} \quad (16)$$

2.2.1.2. Mass transfer

According to the Darcy's Law, the membrane flux (N) can be expressed as the combined influences of the mass transfer coefficient and partial vapor pressure difference across the membrane, as given in Eq. (17):

$$N = K_m \Delta P \quad (17)$$

where K_m is the mass transfer coefficient across the membrane pores, ΔP is the driving pressure difference.

In MD process, the mass transport model of water vapors through the membrane pores is generally described by dusty gas model [21]. This model includes the Knudsen diffusion, molecular diffusion as well as their combinations, the determination of mass transport model in VMD process is dependent on the mean free path of gas molecular (λ_i) and membrane pore size (r). The λ_i can be obtained as follows:

$$\lambda_i = \frac{k_B T_m}{\sqrt{2\pi P_m} \sigma_w^2} \quad (18)$$

where k_B is the Boltzmann constant (1.380×10^{-23} J/K), T_m is mean temperature of membrane pore which is assumed to be equal to that of the membrane surface temperature at the hot side, P_m is mean pressure of membrane pore, σ_w is collision diameter for water vapor (2.641×10^{-10} m).

If r is less than $0.05 \lambda_i$, the Knudsen diffusion is used to describe the mass transport through the membrane pores, the K_m can be calculated as follows:

$$K_m = 1.064 \frac{r\varepsilon}{\tau\delta} \left(\frac{M}{RT_m} \right)^{1/2} \quad (19)$$

where R is the universal gas constant, M is the water molecular mass, τ and δ are the tortuosity and thickness of membrane, respectively.

If r is larger than $50 \lambda_i$, the molecular diffusion is used to describe the mass transport through the membrane pores, the K_m can be calculated as follows:

$$K_m = 0.125 \frac{r^2\varepsilon}{\tau\delta} \left(\frac{MP_m}{\mu_v RT_m} \right) \quad (20)$$

where μ_v is the viscosity of water vapor.

If r is between $0.05 \lambda_i$ and $50 \lambda_i$, both the Knudsen diffusion and molecular diffusion should be considered simultaneously, the K_m can be calculated as follows:

$$K_m = 1.064 \frac{r\varepsilon}{\tau\delta} \left(\frac{M}{RT_m} \right)^{1/2} + 0.125 \frac{r^2\varepsilon}{\tau\delta} \left(\frac{MP_m}{\mu_v RT_m} \right) \quad (21)$$

In this study, the pore size of the membrane is between $0.05 \lambda_i$ and $50 \lambda_i$. Therefore, the Eq. (21) can be chosen to calculate the K_m . The equilibrium vapor pressure is depending on the temperature, concentration and species of the solution on the membrane surface. From the Antoine equation [22], the ΔP can be expressed as follows:

$$\Delta P = P_{\text{sm}} - P_p = (\gamma_{\text{wm}} - 1 - 0.5\gamma_{\text{fm}} - 10\gamma_{\text{fm}}^2) P_{\text{fm}} - P_p = (\gamma_{\text{wm}} (1 - 0.5\gamma_{\text{fm}} - 10\gamma_{\text{fm}}^2)) \exp\left(23.238 - \frac{3841}{T_{\text{fm}} - 45}\right) - P_p \quad (22)$$

where γ_{wm} and γ_{fm} are the mole fraction of water and solute on the membrane surface, P_{fm} is the saturated vapor pressure of pure water at the membrane surface temperature of T_{fm} , P_{sm} is the partial vapor pressure at the membrane surface, P_p is the pressure in the permeate side.

2.2.1.3. Temperature and concentration polarization

In VMD process both mass and heat transfer from the feed side to the permeate side across the boundary layer and membrane. The evaporation of large amount of water molecules on the membrane surface results in the difference in temperature and concentration between the membrane surface and bulk solution. This phenomenon is known as the temperature and concentration polarization effect, and may lead to a significant loss in the driving pressure difference across the membrane. In order to express this phenomenon, the corresponding polarization coefficients are defined as follows:

$$\text{TPC} = \frac{T_{\text{fm}}}{T_f} \quad (23)$$

$$\text{CPC} = \frac{x_{\text{fm}}}{x_f} = \exp\left(\frac{N}{\rho K_f}\right) \quad (24)$$

$$x_f = \frac{x_1 + x_5}{2} \quad (25)$$

where x_f and x_{fm} are the solute concentration of the bulk solution and membrane surface solution, K_f is the solute mass transfer coefficient across the boundary layer, which can be calculated as:

$$\frac{K_f d}{D_L} = \text{Sh} = 0.664 (\text{Re})^{\frac{1}{2}} (\text{Sc})^{\frac{1}{3}} \quad (26)$$

$$\text{Sc} = \frac{\mu}{\rho D_L} \quad (27)$$

where Sh and Sc are the Sherwood and Schmidt numbers, D_L is the diffusion coefficient in the liquid phase.

The temperature polarization effect can be measured by the TPC. The value of TPC ranges from 0 to 1, the larger value of TPC is, the smaller effect of temperature polarization is. As the TPC approaches 1, the temperature between the bulk and the membrane surface solution is almost equivalent and the temperature polarization effect becomes insignificant. The concentration polarization effect can be measured by the CPC. The smaller value of CPC is, the smaller effect of concentration polarization is. As the CPC approaches 1, the concentration between the bulk and membrane surface solution is almost equivalent and the concentration polarization effect becomes insignificant.

2.2.2. Compressor

The compression process of the compressor is approximately for the adiabatic compression, which increases the saturation pressure and temperature of vapor to a higher value. The export state of the compressor is superheated and outlet temperature can be calculated as follows:

$$T_3 = T_2 \left(\frac{P_3}{P_2} \right)^{\frac{k-1}{k}} \quad (28)$$

where T_2 and T_3 are the inlet and outlet temperature of the compressor, respectively, P_2 and P_3 are the inlet and outlet pressure of the compressor, respectively, k is the polytropic exponent of the compression process.

The actual power consumption of compressor can be calculated as follows [23]:

$$W = F_2 \frac{k \times R \times T_2}{\eta_{th} \times \eta_{me} (k-1)} \left[\left(\frac{P_3}{P_2} \right)^{\frac{k-1}{k}} - 1 \right] \quad (29)$$

where η_{th} is the thermal efficiency of the compressor 76%, η_{me} is the mechanical efficiency of the compressor 80%.

2.2.3. Heat exchanger

The energy balance equation of the heat exchanger is given by:

$$F_5 (h_6 - h_5) = F_2 (h_3 - h_4) \quad (30)$$

where h_5 and h_6 are the specific enthalpy of the solution at the cold side inlet and outlet of heat exchanger, h_4 is the specific enthalpy of the condensate water at the hot side outlet of heat exchanger.

$$A = \frac{F_2 (h_3 - h_4)}{U \Delta t_{LMTD}} \quad (31)$$

where A is the heat transfer area, U is the overall coefficient of heat transfer, Δt_{LMTD} is the logarithmic mean temperature difference of heat exchanger, it can be given by:

$$\Delta t_{LMTD} = \frac{(T_3 - T_6) - (T_4 - T_5)}{\ln \left(\frac{T_3 - T_6}{T_4 - T_5} \right)} \quad (32)$$

After the mathematical models of the proposed system are presented, the corresponding numerical simulation can be realized adopting the platform of Matlab with the balance equations solved iteratively, the schematic of solution procedure of the mathematical models is shown in Fig. 3.

3. Model validation

The mathematical models applied in the proposed system have been validated using the experimental data obtained from the literature [20], the concentration of the NaCl solution and permeate-side absolute pressure are kept at 4.5% and 4 kPa both in the experiments and the simulation work. Fig. 4 shows the comparison of the experimental and simulated membrane flux with the feed velocity in the range of 0.2 to 1.0 m/s and the feed temperature in the range of 40°C to 60°C, it is clear that the simulated curve of membrane flux is close to the experimental values under the same operation conditions, and the relative error is found to be within 12.5%. Therefore, the currently established models can guarantee good accuracy in assessing the performance of the proposed system.

4. Results and discussion

For the whole distillation process, temperature and concentration polarization effects caused by the liquid boundary layer are the major barriers inhibiting mass and heat transfer from the bulk solution to the membrane surface. But beyond that, the BPE, transmembrane resistance and heat transfer temperature difference of heat exchanger also have different contributions to the heat transfer and conversion within the proposed system. In the following sections, the working mechanisms of them at various operating parameters are investigated and discussed comprehensively.

4.1. Analysis of temperature polarization effect

Figs. 5 and 6 show variations in TPC, temperature of bulk solution (T_f) and temperature on the membrane surface (T_{im}) as a function of the feed concentration (1%–25%) and feed temperature (75°C–90°C), at the conditions of feed velocity of 1.0 m/s, and permeate-side absolute pressure of 30 kPa. As depicted, the TPC increases with the increase of the feed concentration, but the difference between T_f and T_{im} decreases with the increase of the feed concentration, the reason is that the increase of the feed concentration increases the viscosity of the solution and decreases the activity coefficient of the water molecules, which reduces the partial vapor pressure and evaporation rate of water molecules on the membrane surface, thereby increasing the temperature on the membrane surface and weakening temperature polarization effect, then results in the decrease of the difference between T_f and T_{im} . In addition, it is observed that the TPC decreases with the increase of feed temperature, while the feed concentration is maintained invariable. The increase

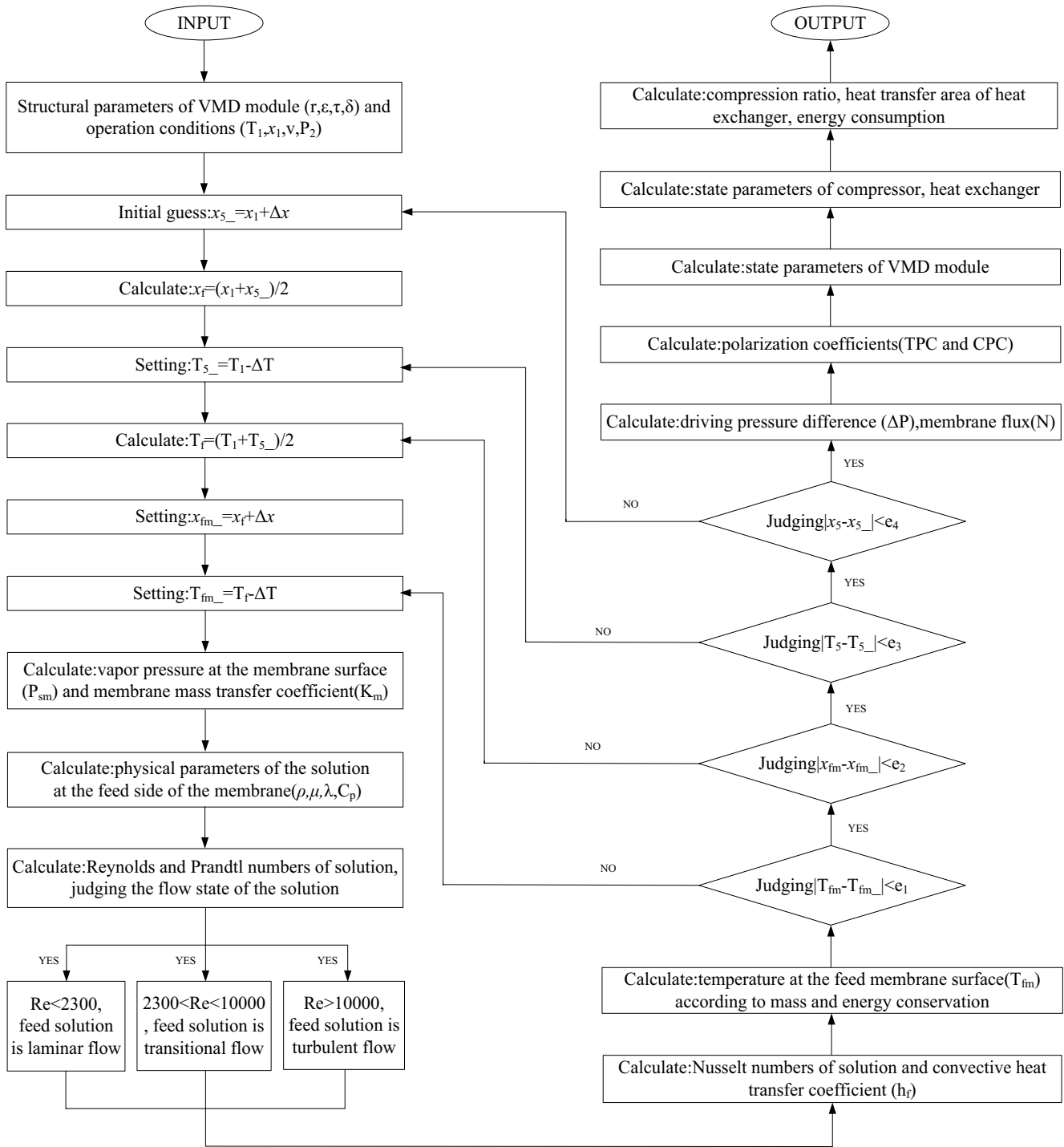


Fig. 3. Schematic of solution procedure of the mathematical models of the proposed system.

of feed temperature increases the activity and energy of all molecules in the solution, which is conducive to increase the temperature both of bulk and membrane surface solution. However, the increase of saturated vapor pressure on the membrane surface makes more water molecules evaporate and take away the latent heat. As a result, the rising rate of membrane surface temperature is lower than that of bulk solution, which results in strengthening the temperature

polarization effect, thus decreasing the TPC and increasing temperature difference between T_f and T_{fm} .

Figs. 7 and 8 show variations in TPC, temperature of bulk solution (T_f) and temperature on the membrane surface (T_{fm}) as a function of the feed concentration (1%–25%) and feed velocity (0.8–1.4 m/s), at the conditions of feed temperature of 85°C, and permeate-side absolute pressure of 45 kPa. It is found that higher feed velocity results in more

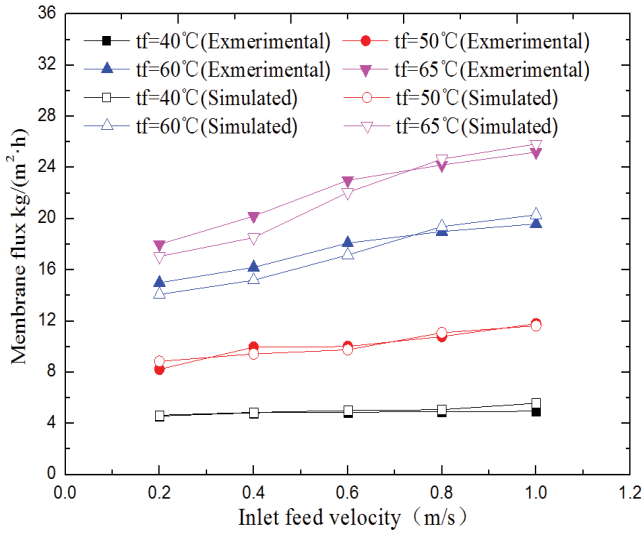


Fig. 4. Comparison of experimental and simulated values.

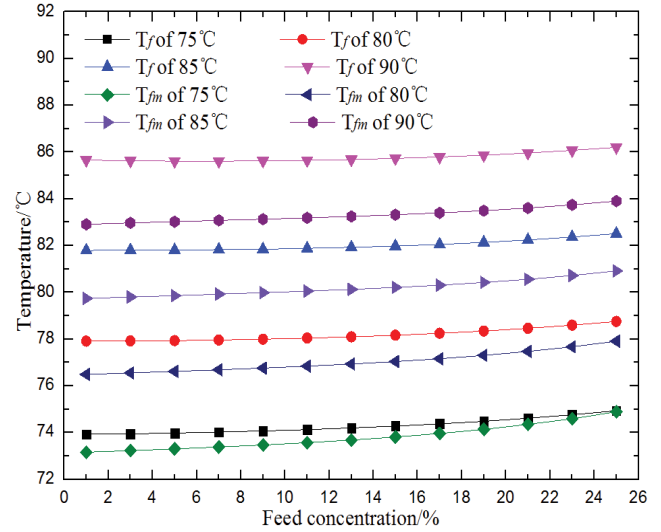


Fig. 6. Variations in T_f and T_{fm} as a function of feed concentration and feed temperature.

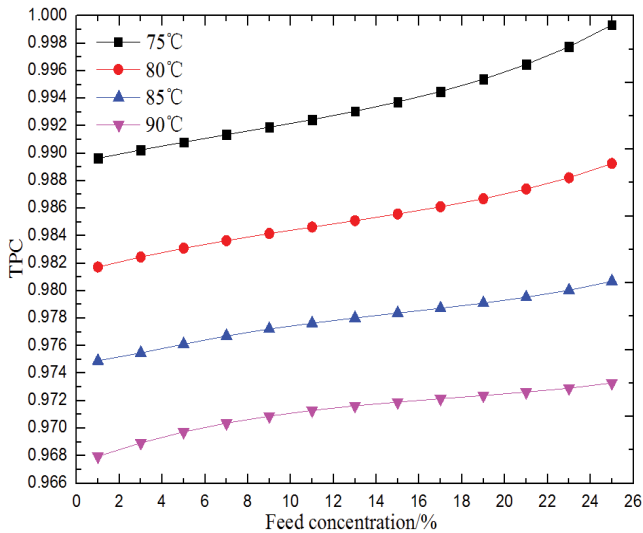


Fig. 5. Variations in TPC as a function of feed concentration and feed temperature.

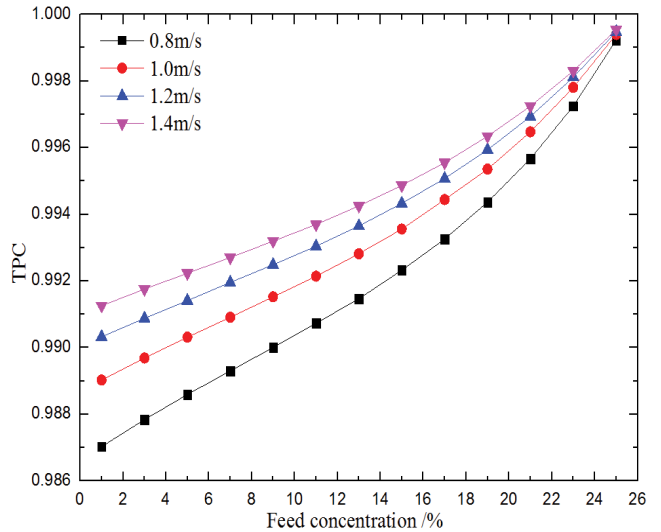


Fig. 7. Variations in TPC as a function of feed concentration and feed velocity.

intensive the turbulence and larger Reynolds number, which can also decrease the boundary layer thickness and increase the convection heat transfer coefficients, and weaken the temperature polarization effects, results in the increase of TPC and decrease of the temperature difference between T_f and T_{fm} .

Figs. 9 and 10 show variations in TPC, temperature of bulk solution (T_f) and temperature on the membrane surface (T_{fm}) as a function of the feed concentration (1%–25%) and permeate-side absolute pressure (30–45 kPa), at the conditions of feed temperature of 85°C, and feed velocity of 1.0 m/s. Increasing permeate-side absolute pressure does not directly change the flow state of the solution, but it can lead to the decrease of driving pressure difference and evaporation rate of water molecules, which decreases temperature polarization effect and the difference between T_f and T_{fm} .

4.2. Analysis of concentration polarization effect

Figs. 11–13 show variations in CPC and concentration difference between bulk and membrane surface solution (ΔC) as a function of feed concentration (1%–25%) at various operating conditions. Based on the analysis in section 4.1, the increase of feed concentration increases the viscosity of the solution and decreases the diffusion rate of water molecules through the boundary layer to the membrane surface, and decreases the evaporation rate of water molecules on the membrane surface, and the increase rate of solution concentration on the membrane surface due to evaporation of water molecules will decrease, and the concentration polarization phenomenon will decrease, so the value of CPC will decrease. However, the value of ΔC shows a rise first followed

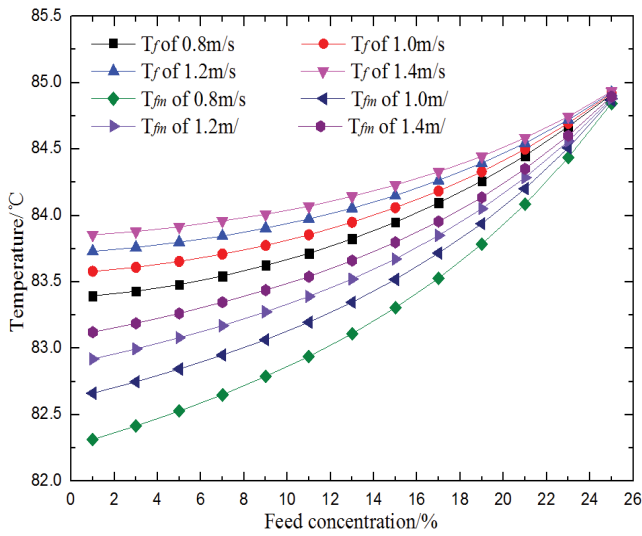


Fig. 8. Variations in T_f and T_{fm} as a function of feed concentration and feed velocity.

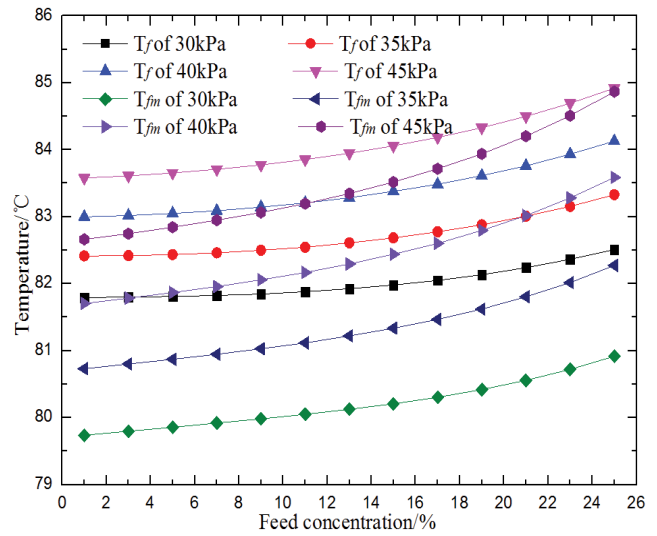


Fig. 10. Variations in T_f and T_{fm} as a function of feed concentration and permeate-side absolute pressure.

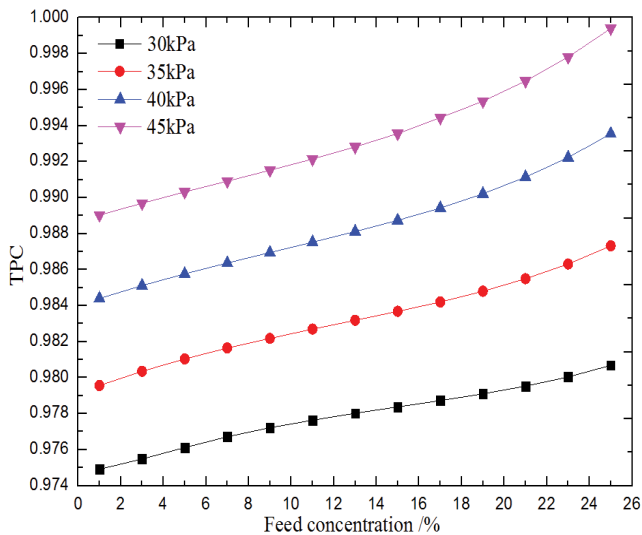


Fig. 9. Variations in TPC as a function of feed concentration and permeate-side absolute pressure.

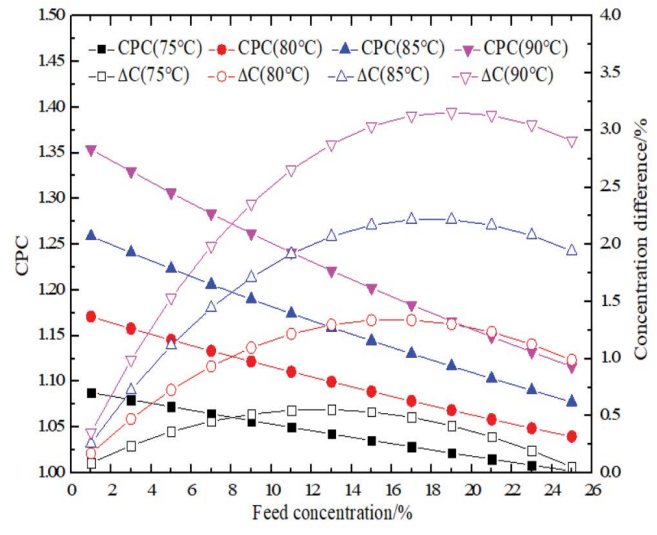


Fig. 11. Variations in CPC and concentration difference (ΔC) as a function of feed concentration and feed temperature.

by a decline with the increase of feed concentration, when the feed concentration is the lowest, that is, pure water, the value of ΔC will be 0°C . When the feed concentration reaches the maximum, there will be no water vapor molecules passing through the membrane pore, and the increasing trend of the solution concentration on the membrane surface due to water evaporation will disappear. The concentration of the membrane surface solution is almost the same as that of the bulk solution, and the value of CPC is close to 1. Therefore, there will be a peak in the value of ΔC . It also can be seen from Fig. 11 that, increasing feed temperature promotes the transfer both of water and solute molecules through the boundary layer to the membrane surface, and water molecules evaporate through membrane pores instead of solute molecules, causing a large number of solute molecules to accumulate on

the membrane surface, which strengthens the concentration polarization effect and increases the values of CPC and ΔC . Moreover, increasing feed velocity can directly affect concentration polarization effect by changing the solution flow state and reducing the concentration boundary layer thickness, thus decreasing the values of CPC and ΔC . Finally, increasing permeate-side absolute pressure reduces the driving pressure difference on both sides of membrane and evaporation rate of water molecules on the membrane surface, so as to weaken the concentration polarization effect, the values of CPC and ΔC decline correspondingly.

4.3. Analysis of compressor power

The temperature and concentration of the membrane surface solution will change during the concentration

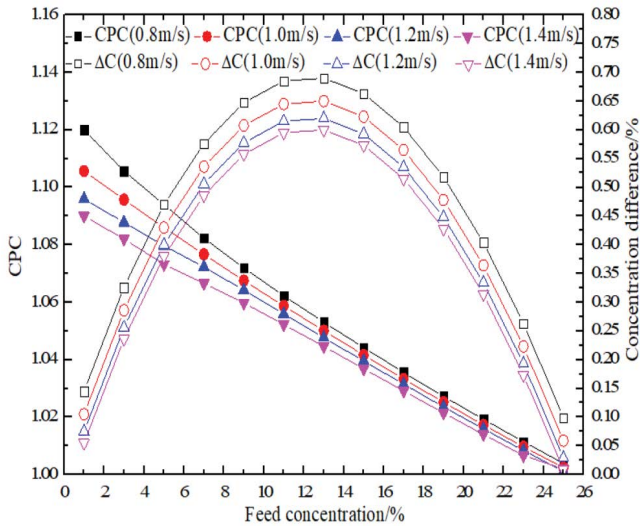


Fig. 12. Variations in CPC and concentration difference (ΔC) as a function of feed concentration and feed velocity.

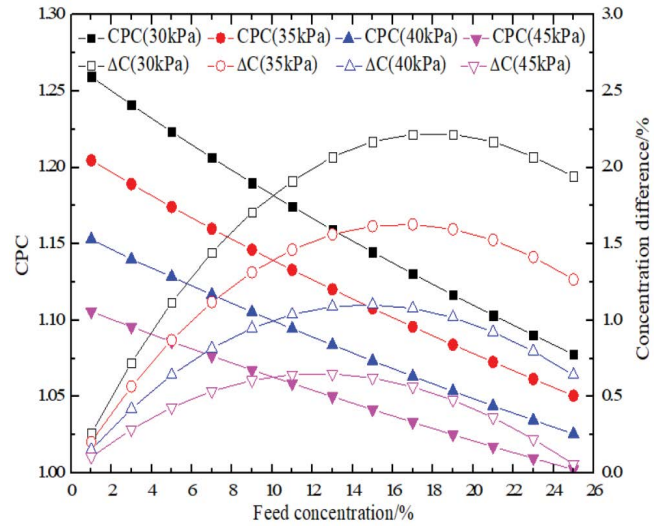


Fig. 13. Variations in CPC and concentration difference (ΔC) as a function of feed concentration and permeate-side absolute pressure.

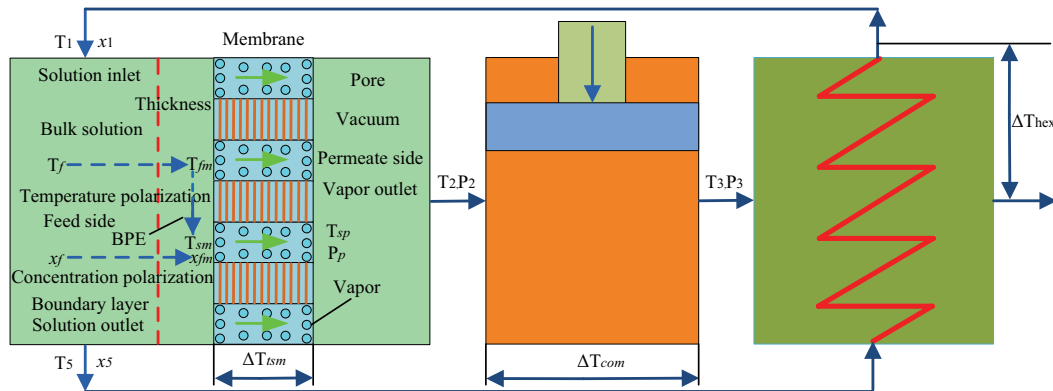


Fig. 14. Schematic diagram of the mass and heat transfer process of the proposed system.

process for the proposed system, which will reduce the driving pressure difference and water production performance of the membrane. Therefore, in order to ensure stable water production, it can be achieved by improving the overall energy of the feed solution, which will increase the power of the compressor. As the compressor is the key component of the proposed system, its power consumption has a significant impact on the energy consumption of the whole system. Generally, the compressor power is determined by both of the vapor mass flow rate and the compression ratio, and the saturated temperature difference between inlet and outlet of the compressor (ΔT_{com}) has positive correlation with compression ratio under the condition that the inlet of the compressor maintains the uniform pressure. Fig. 14 shows the schematic diagram of the mass and heat transfer process of the proposed system, and Fig. 15 shows the corresponding T-S diagram. The point *a* is the state at which the feed solution is preheated to the required temperature of T_1 , the point *b* is the state of the bulk solution, ΔT_{eva} is the temperature

difference between *a* and *b* due to the large heat loss caused by evaporation in VMD module. The point *c* is the state of the membrane surface solution, ΔT_{tpe} is the temperature difference between *b* and *c* due to the temperature polarization effect. The point *d* is the state of the vapors evaporated from the membrane surface solution at the hot side, the T_{sm} is the saturated temperature of pure water corresponding to the P_{sm} , the temperature difference between T_{fm} and T_{sm} can be expressed as ΔT_{BPE} , which is caused by the BPE phenomenon. The point *e* is the state of the vapors transferred from the hot side to the permeate side across the membrane, the driving pressure difference is caused by the temperature difference (ΔT_{ism}) between T_{sm} and T_{sp} , it is pointed out that the T_{sp} is saturated temperature corresponding to the P_p and the transmembrane transport process of the vapors can be modeled as nearly isothermal expansion from P_{sm} to P_p [24]. The point *f* is the state of the vapors compressed by the steam compressor. The point *g* is the state of the saturated vapor corresponding to the P_3 . The point *h* is the state of

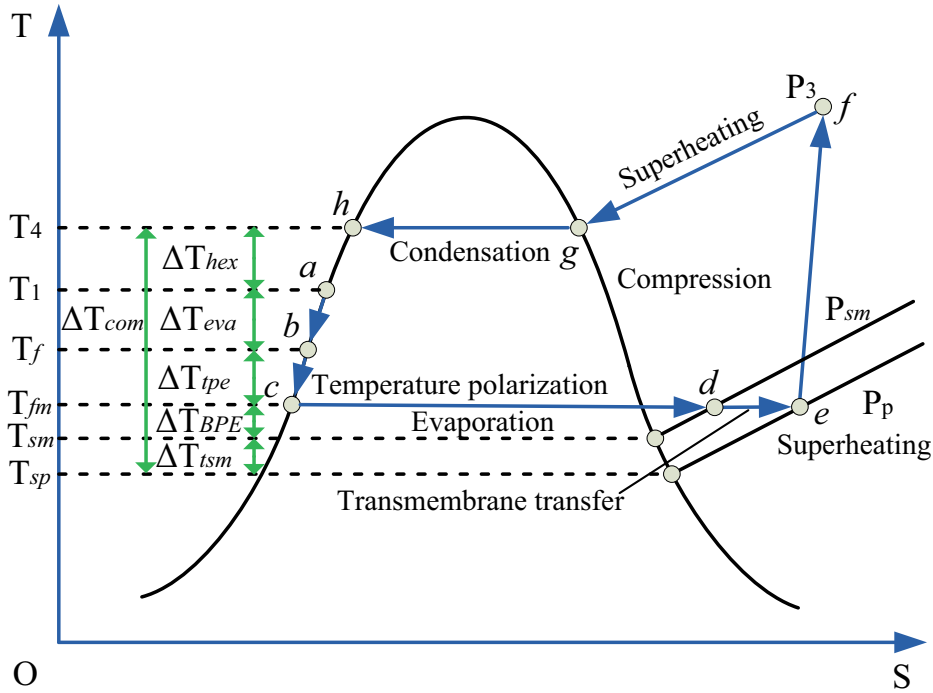


Fig. 15. T-S diagram of the proposed system.

the condensed water after releasing latent heat in the heat exchanger, and ΔT_{hex} is the heat transfer temperature difference of the heat exchanger. Therefore, there are many factors such as temperature polarization resistance, concentration polarization resistance, BPE, transmembrane resistance and heat transfer temperature difference of heat exchanger determining the value of ΔT_{com} , thereby affecting the compression ratio and power consumption of the compressor. The ΔT_{com} can be expressed as follows:

$$\begin{aligned} (T_1 - T_f) + (T_f - T_{fm}) + (T_{fm} - T_{sm}) + (T_{sm} - T_{sp}) + (T_{sp} + \Delta T_{com}) = \\ \Delta T_{eva} + \Delta T_{tpe} + \Delta T_{BPE} + \Delta T_{tsm} + \Delta T_{hex} + T_1 \Rightarrow \Delta T_{com} = \Delta T_{eva} + (33) \\ \Delta T_{tpe} + \Delta T_{BPE} + \Delta T_{tsm} + \Delta T_{hex} \end{aligned}$$

The main objective of this part is to investigate the effects of critical factors on compressor power at various operating conditions, while the driving pressure difference, membrane flux and ΔT_{hex} are fixed at a constant value of 7.3 kPa, 10 kg/(m² h) and 4°C, respectively. Fig. 16a shows variations in ΔT_{eva} , ΔT_{tpe} , ΔT_{BPE} , ΔT_{tsm} , ΔT_{hex} and ΔT_{com} as a function of the feed concentration, at the conditions of feed velocity of 1.0 m/s, and permeate-side absolute pressure of 35 kPa. Apparently, it is found that the ΔT_{com} rises significantly due to the increase of the feed concentration, which is mainly attributed to the following three parts. First, the ΔT_{BPE} is significantly increased when the feed concentration is higher. Although the vapor production is through evaporation on the membrane surface rather than boiling, the increase of solution concentration leads to the BPE, resulting in a reduction of vapor partial pressure at the membrane surface. Therefore, the solution on the membrane surface need to be heated to a higher temperature

to overcome the BPE phenomenon. Second, since the heat of the solution on the membrane surface is transferred from the bulk solution through the thermal boundary layer, only higher temperature of the bulk solution can guarantee the increase of the membrane surface temperature in order to achieve a constant vapor production, which will aggravate the temperature polarization effect and increase the value of ΔT_{tpe} . Third, the ΔT_{eva} is the measurement of how much thermal energy is lost by evaporation from the feed solution as both of the heat loss to the environment and conduction heat loss through the membrane are negligible. Increasing the feed concentration makes the temperature of membrane surface and bulk solution higher in order to maintain the same membrane flux, leading to an increase of the heat carried by the evaporated vapor and the value of ΔT_{eva} .

Fig. 16b shows variations in ΔT_{eva} , ΔT_{tpe} , ΔT_{BPE} , ΔT_{tsm} , ΔT_{hex} and ΔT_{com} as a function of the feed concentration, at the conditions of feed velocity of 1.0 m/s, and permeate-side absolute pressure of 40 kPa. The explanation for the ΔT_{com} decreases with increasing permeate-side absolute pressure from 35 to 40 kPa is as follows. The increase of permeate-side absolute pressure leads to a significant reduction of ΔT_{tsm} from 4.48°C to 4.06°C at a fixed driving pressure difference of 7.3 kPa, but the values of ΔT_{eva} , ΔT_{tpe} and ΔT_{BPE} change little. According to the above analysis of TPC and CPC given in Section 4.1 and 4.2, when the feed concentration is maintained unchanged, the increase of permeate-side absolute pressure weakens temperature and concentration polarization effect, but increases the heat loss of bulk solution by evaporation, resulting in the decrease of the ΔT_{BPE} and ΔT_{tpe} , and the increase of the ΔT_{eva} .

Fig. 16c shows variations in ΔT_{eva} , ΔT_{tpe} , ΔT_{BPE} , ΔT_{tsm} , ΔT_{hex} and ΔT_{com} as a function of the feed concentration, at

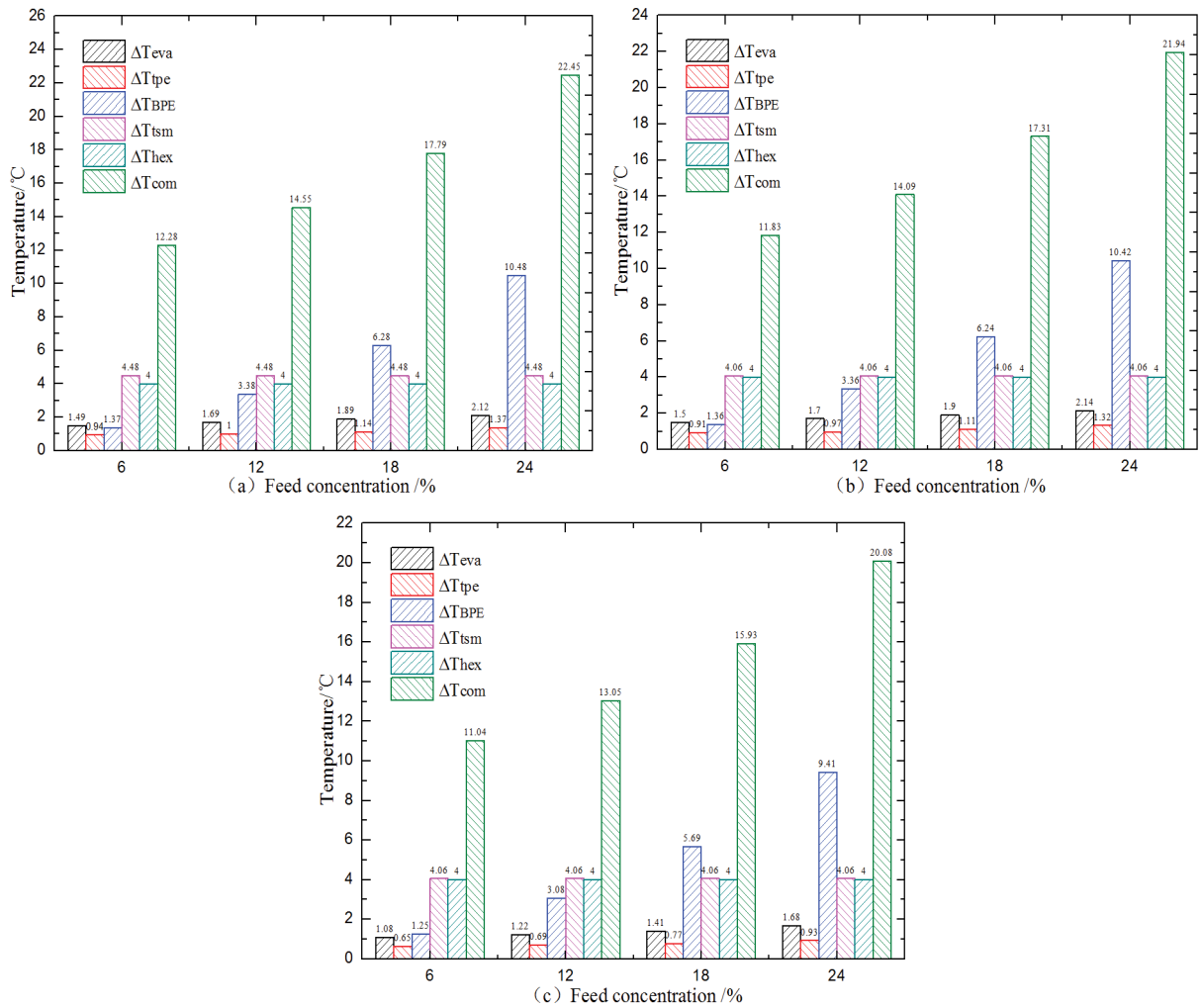


Fig. 16. Variations in ΔT_{eva} , ΔT_{tpe} , ΔT_{BPE} , ΔT_{tsm} , ΔT_{hex} and ΔT_{com} as a function of feed concentration at various process conditions, (a) $v = 1.0$ m/s, $P_p = 35$ kPa; (b) $v = 1.0$ m/s, $P_p = 40$ kPa and (c) $v = 1.4$ m/s, $P_p = 40$ kPa.

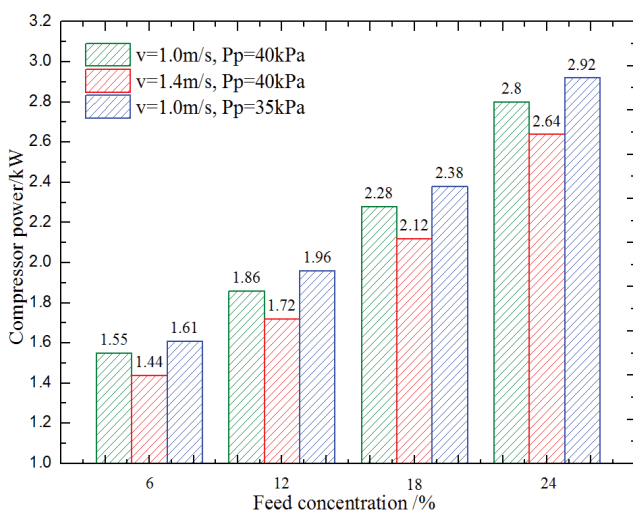


Fig. 17. Variations in compressor power as a function of feed concentration at various conditions.

the conditions of feed velocity of 1.4 m/s, and permeate-side absolute pressure of 40 kPa. It can be seen that the ΔT_{com} decreases with increasing feed velocity from 1.0 to 1.4 m/s. This happens due to the reduction of the boundary layer thickness, followed by the decrease of temperature and concentration polarization effect and heat loss of bulk solution by evaporation, significantly influences the ΔT_{BPE} , ΔT_{tpe} and ΔT_{eva} . It should be noted that the ΔT_{tsm} keeps constant at 4.06°C based on the fixed permeate-side absolute pressure and driving vapor pressure.

Fig. 17 shows variations in compressor power as a function of the feed concentration at various conditions. As it is well known, the compressor power is influenced by both compression ratio and ΔT_{com} . In addition, it depends on different operating conditions. Apparently, it can be observed that the total compressor power rises significantly due to the increase of the feed concentration and the decrease of feed velocity and permeate-side absolute pressure, which is mainly attributed to the increase of the ΔT_{com} as well as the compression ratio of the compressor. For example, an increase in feed velocity from 1.0 to 1.4 m/s at a constant

Table 2
Comparison of STEC between the proposed system and solar powered MD system

Membrane material	Pore size (um)	Membrane area (m ²)	Feed temperature (°C)	Membrane flux (kg/m ² h)	STEC (kWh/m ³)	
					This study	Reference
PTFE	0.2	8.5	65	2.35	85	140

feed concentration of 12% and permeate-side absolute pressure of 40 kPa results in a reduction of compressor power from 1.86 to 1.72 kW. Similarly an increase in permeate-side absolute pressure from 35 to 40 kPa at a constant feed concentration of 12% and feed velocity of 1.0 m/s is found to result in a reduction of compressor power from 1.96 to 1.86 kW.

4.4. Analysis of energy saving performance

The STEC for the proposed system is defined as the amount of energy consumption used to produce 1 m³ of distillate product, it can be defined as:

$$\text{STEC} = \frac{W}{NA_f} \quad (34)$$

The STEC is important to evaluate the thermal efficiency of the proposed system, the energy consumption of the proposed system mainly includes the power consumption of the circulation pump, vacuum pump and compressor. For simplicity, the thermal energy loss to the ambient of the components in the system have not been accounted for, and the main energy consumption is the power consumption of the compressor. In order to further investigate the energy saving performance of the proposed system in solution concentration process, a solar powered MD system reported in [25] is selected as comparison, in which the energy used for heating the solution is totally supplied by the solar collector system. Table 2 compares the STEC of different systems under the same conditions of membrane characteristics, feed temperature and membrane flux, the STEC of solar powered MD system is calculated based on the experimental data, and the STEC of the proposed system is directly taken from simulation data. It can be seen from Table 2 that the STEC of the proposed system was less than that of solar powered MD system by 39.3%, which indicates that the latent heat recovery of secondary steam based on MVR is important to achieve a low STEC for the proposed system. Therefore, the proposed system recovering the latent heat of vaporization has a better energy efficiency and reliability than the solar powered MD system.

5. Conclusions

In this work, a comprehensive design model is developed to predict the characteristics of a combined system of VMD and MVR. Taking the sodium chloride solution as the treated solution, detailed mathematical models based on the mass and energy balance in each part of the system are established.

According to the simulation results, the primary conclusions are listed as follows:

- The influences of operating parameters such as feed temperature, feed velocity, feed concentration and permeate-side absolute pressure on temperature and concentration polarization effects are evaluated. It is found that TPC increases with the rise of feed concentration, feed velocity and permeate-side absolute pressure, but it decreases with the rise of feed temperature. However, CPC increases with the rise of feed temperature, but it decreases with the rise of feed concentration, feed velocity and permeate-side absolute pressure.
- The influencing mechanisms of temperature polarization effect, concentration polarization effect, BPE, transmembrane resistance and heat transfer temperature difference of heat exchanger on compressor power at various operating conditions are obtained. It is observed that the contributions of the above critical factors on the compressor power are different at various operating conditions. A decrease of compressor power is evidenced, which can be achieved through reducing the impact of critical factors such as temperature polarization, concentration polarization and BPE on the distillation process by adjusting operating conditions.
- A comparison of the proposed system against the solar powered MD system of using solar as a heat source shows good energy saving in the concentration process of solution, the STEC is 85 kWh/m³ at the conditions of feed temperature of 65°C and membrane flux of 2.35 kg/m² h, which is less than that of solar powered MD system by 39.3%.

Symbols

A	—	Heat transfer area of heat exchanger, m ²
A_f	—	Effective area of inner surface of hollow fiber membrane, m ²
A_{im}	—	Effective heat transfer area across the membrane, m ²
C_p	—	Heat capacity of feed solution, kJ/(kg °C)
d^p	—	Inner fiber diameter, mm
D	—	Outer fiber diameter, mm
D_L	—	Diffusion coefficient of the solute in solvent, m ² /s
F	—	Mass flow rate, kg/s
h	—	Enthalpy, kJ/kg
h_f	—	Heat transfer coefficient at the feed solution boundary layer, W/(m ² °C)
k	—	Polytropic exponent of the compression process, 1.33

k_B	— Boltzmann constant
k_g	— Thermal conductivity of the gas mixture, W/(m °C)
k_m	— Membrane thermal conductivity, W/(m °C)
k_p	— Thermal conductivity of the membrane material, W/(m °C)
K_f	— Solute mass transfer coefficient across thermal boundary layer, m/s
K_m	— Mass transfer coefficient across the membrane pores, kg/(m ² s Pa)
l	— Fiber length, m
M	— Water molecular mass
n	— Number of fibers
N	— Membrane flux, kg/(m ² h)
Nu	— Nusselt number
P_m	— Mean pressure of membrane pore
P_p	— Pressure in the permeate side, kPa
Pr	— Prandtl number
Q_f	— Heat transfers from the bulk solution to the membrane surface through the boundary layer, W
Q_m	— Heat transfers from the membrane surface to permeate side through the membrane, W
r	— Pore size, μm
R	— Universal gas constant, 8.314 J/(mol °C)
Re	— Reynolds number
Sc	— Schmidt number
Sh	— Sherwood number
T_f	— Temperature of the feed bulk solution, °C
T_{fm}	— Temperature at the feed membrane surface, °C
T_m	— Mean temperature of membrane pore, °C
T_{pm}	— Temperature at the permeation membrane surface, °C
U	— Overall coefficient of heat transfer of heat exchanger, W/(m ² °C)
W	— Power, W
x	— Solute mass fraction of the solution
ΔH	— Latent heat of vaporization, kJ/kg
Δt_{LMTD}	— Logarithmic mean temperature difference of heat exchanger, °C

Abbreviations

AGMD	— Air gap membrane distillation
BPE	— Boiling point elevation
CPC	— Concentration polarization coefficient
DCMD	— Direct contact membrane distillation
MVR	— Mechanical vapor recompression
PTFE	— Polytetrafluoroethylene
STEC	— Specific thermal energy consumption
SGMD	— Sweeping gas membrane distillation
TPC	— Temperature polarization coefficient
VMD	— Vacuum membrane distillation

Greek letters

γ	— Mole fraction
δ	— Thickness, mm
ε	— Porosity
η	— Efficiency

λ	— Thermal conductivity of feed solution, W/(m °C)
μ	— Dynamic viscosity of feed solution, Pa s
ρ	— Density, kg/m ³
τ	— Tortuosity

Subscripts

com	— Compressor
eva	— Evaporation
f	— Feed side
f_m	— Membrane surface in feed side
g	— Gas
hex	— Heat exchanger
m	— Membrane
me	— Mechanical efficiency
p	— Pore, pressure, permeate side
pm	— Membrane surface in permeate side
sm	— Saturated state at the membrane surface
sp	— Saturated state in permeate side
th	— Thermal
tpe	— Temperature polarization effect
tsm	— Transmembrane
vac	— Vacuum pump

Acknowledgement

The authors would like to acknowledge the financial support from the Fundamental Research Funds for the Central Universities (NO.NP2018107) and Postgraduate Research & Practice Innovation Program of Jiangsu Province (KYCX19_0183).

References

- [1] W.F. He, D. Han, C. Yue, W.H. Pu, A parametric study of a humidification dehumidification (HDH) desalination system using low grade heat sources, *Energy Convers. Manage.*, 105 (2015) 929–937.
- [2] Z.X. Liang, L. Zhang, Z.Q. Yang, X.N. Cheng, G. Pu, J.Y. Ran, The effect of solid particles on the evaporation and crystallization processes of the desulfurization wastewater droplet, *Appl. Therm. Eng.*, 134 (2018) 141–151.
- [3] S. Srisurichan, R. Jiratananon, A.G. Fane, Mass transfer mechanisms and transport resistances in direct contact membrane distillation process, *J. Membr. Sci.*, 277 (2006) 186–194.
- [4] F. Jia, J.F. Li, J.L. Wang, Y.L. Sun, Removal of strontium ions from simulated radioactive wastewater by vacuum membrane distillation, *Ann. Nucl. Energy*, 103 (2017) 363–368.
- [5] L.D. Tijing, Y.C. Woo, M.A.H. Johir, J.-S. Choi, H.K. Shon, A novel dual-layer bicomponent electrospun nanofibrous membrane for desalination by direct contact membrane distillation, *Chem. Eng. J.*, 256 (2014) 155–159.
- [6] M. Khayet, C. Cojocaru, A. Baroudi, Modeling and optimization of sweeping gas membrane distillation, *Desalination*, 287 (2012) 159–166.
- [7] F.F. Shao, C.Q. Hao, L. Ni, Y.F. Zhang, R.H. Du, J.Q. Meng, C.F. Xiao, Experimental and theoretical research on N-methyl-2-pyrrolidone concentration by vacuum membrane distillation using polypropylene hollow fiber membrane, *J. Membr. Sci.*, 452 (2014) 157–164.
- [8] Z.L. Chen, D. Rana, T. Matsuura, Y.F. Yang, C.Q. Lan, Study on the structure and vacuum membrane distillation performance of PVDF composite membranes: I. Influence of blending, *Sep. Purif. Technol.*, 133 (2014) 303–312.

- [9] D.L.M. Mendez, C. Castel, C. Lemaitre, E. Favre, Improved performances of vacuum membrane distillation for desalination applications: materials vs process engineering potentialities, *Desalination*, 452 (2019) 208–218.
- [10] H.Y. Zhang, B.B. Li, D. Sun, X.L. Miao, Y.L. Gu, SiO₂-PDMS-PVDF hollow fiber membrane with high flux for vacuum membrane distillation, *Desalination*, 429 (2018) 33–43.
- [11] F. Banat, N. Jwaied, M. Rommel, J. Koschikowski, M. Wiegand, Desalination by a “compact SMADES” autonomous solarpowered membrane distillation unit, *Desalination*, 217 (2007) 29–37.
- [12] Q.M. Ma, A. Ahmadi, C. Cabassud, Direct integration of a vacuum membrane distillation module within a solar collector for small-scale units adapted to seawater desalination in remote places: design, modeling & evaluation of a flat-plate equipment, *J. Membr. Sci.*, 564 (2018) 617–633.
- [13] P. Boutikos, E.Sh. Mohamed, E. Mathioulakis, V. Belessiotis, A theoretical approach of a vacuum multi-effect membrane distillation system, *Desalination*, 422 (2017) 25–41.
- [14] Y. Kansha, A. Kishimoto, A. Tsutsumi, Application of the self-heat recuperation technology to crude oil distillation, *Appl. Therm. Eng.*, 43 (2012) 153–157.
- [15] Y. Zhou, C.J. Shi, G.Q. Dong, Analysis of a mechanical vapor recompression wastewater distillation system, *Desalination*, 353 (2014) 91–97.
- [16] D. Tong, X.Z. Wang, M. Ali, C.Q. Lan, Y. Wang, E. Drioli, Z.H. Wang, Z.L. Cui, Preparation of Hyflon AD60/PVDF composite hollow fiber membranes for vacuum membrane distillation, *Sep. Purif. Technol.*, 157 (2014) 1–8.
- [17] W.F. He, D. Han, L.N. Xu, C. Yue, W.H. Pu, Performance investigation of a novel water–power cogeneration plant (WPCP) based on humidification dehumidification (HDH) method, *Energy Convers. Manage.*, 110 (2016) 184–191.
- [18] W.F. He, L. Huang, J.R. Xia, W.P. Zhu, D. Han, Y.K. Wu, Parametric analysis of a humidification dehumidification desalination system using a direct-contact dehumidifier, *Int. J. Therm. Sci.*, 120 (2017) 31–40.
- [19] J.I. Mengual, M. Khayet, M.P. Godino, Heat and mass transfer in vacuum membrane distillation, *Int. J. Heat Mass Transfer*, 47 (2004) 865–875.
- [20] Y.-D. Kim, K. Thu, S.-H. Choi, Solar-assisted multi-stage vacuum membrane distillation system with heat recovery unit, *Desalination*, 367 (2015) 161–171.
- [21] C.-K. Chiam, R. Sarbatly, Study of the rectangular cross-flow flat-sheet membrane module for desalination by vacuum membrane distillation, *Chem. Eng. Process. Process Intensif.*, 102 (2016) 169–185.
- [22] J.L. Xu, Y.B. Singh, G.L. Amy, N. Ghaffour, Effect of operating parameters and membrane characteristics on air gap membrane distillation performance for the treatment of highly saline water, *J. Membr. Sci.*, 512 (2016) 73–82.
- [23] D. Han, W.F. He, C. Yue, W.H. Pu, L. Liang, Analysis of energy saving for ammonium sulfate solution processing with self-heat recuperation principle, *Appl. Therm. Eng.*, 73 (2014) 641–649.
- [24] H.W. Chung, J. Swaminathan, D.M. Warsinger, J.H. Lienhard V, Multistage vacuum membrane distillation (MSVMD) systems for high salinity applications, *J. Membr. Sci.*, 497 (2016) 128–141.
- [25] R.G. Raluy, R. Schwantes, V.J. Subiela, B. Peñate, G. Meliána, J.R. Betancort, Operational experience of a solar membrane distillation demonstration plant in Pozo Izquierdo-Gran Canaria Island (Spain), *Desalination*, 290 (2012) 1–13.